12th International Symposium on Turbulence and Shear Flow Phenomena (TSFP12)
Osaka, Japan, July 19–22, 2022

# SYMMETRY BREAKING AND TURBULENCE IN OSCILLATORY FLOW THROUGH A HEXAGONAL SPHERE PACK

**Lukas Unglehrt**
Professorship of Hydromechanics
Technical University of Munich
Arcisstr. 21, 80335 Munich, Germany
lukas.unglehrt@tum.de

**Michael Manhart**
Professorship of Hydromechanics
Technical University of Munich
Arcisstr. 21, 80335 Munich, Germany
michael.manhart@tum.de

## ABSTRACT

The appearance of turbulence in oscillatory flow through a hexagonal sphere pack was investigated by means of direct numerical simulation. The Reynolds numbers lie between 26.9 and 297 and the Womersley number is 31.62. We characterised the flow state based on instantaneous velocity fields and the time series of the superficial velocity. The velocity fields were decomposed into symmetric and antisymmetric components with respect to the symmetries of the sphere pack. Based on the temporal evolution of the kinetic energy of the antisymmetric components, it is possible to distinguish between laminar, transitional and turbulent flow. Finally, the velocity fields were decomposed with respect to the average over the realisations that can be obtained by applying the symmetries of the hexagonal sphere pack. For the turbulent flow case, a significant scale separation between the average and fluctuating velocity fields is observed.

## INTRODUCTION

Oscillatory porous media flow occurs in wave-induced transport processes in coral reefs (Lowe *et al.*, 2008) or in the sediment bed; moreover, it could be of interest to enhance solute transport in chemical reactors (Crittenden *et al.*, 2005). Other applications include for example wave-induced flow through rubble-mound breakwaters (van Gent, 1993; Hall *et al.*, 1995). In order to describe these transport processes, it is essential to know whether the pore scale flow is turbulent, as turbulence is associated with strong mixing.

Starting with Dybbs & Edwards (1984), the microscale behaviour of stationary turbulent flow through regular and random sphere packs has been studied numerically (e.g. Hill & Koch, 2002; He *et al.*, 2019; Sakai & Manhart, 2020) and experimentally (e.g. Patil & Liburdy, 2012, 2013). Four flow regimes are commonly distinguished (Dybbs & Edwards, 1984) depending on the Reynolds number: i) linear flow, ii) steady nonlinear flow, iii) unsteady nonlinear flow and iv) chaotic / turbulent flow. The transition to turbulent flow generally occurs for Reynolds numbers around 120 (Fand *et al.*, 1987). In regular sphere packs, the emergence of chaotic and turbulent flow can be related to symmetry breaking bifurcations that occur around a Reynolds number of 100 (Hill & Koch, 2002) or for $138 < Re < 209$ (Sakai & Manhart, 2020).

Experimental studies of turbulent oscillatory porous media flow have been performed with a focus on the behaviour of bulk flow quantities (van Gent, 1993; Hall *et al.*, 1995; Losada *et al.*, 1995; Pamuk & Özdemir, 2014; Bağcı *et al.*, 2016) or on the processes at the interface between the porous medium and a free flow (Shigematsu *et al.*, 2018). On the other hand, numerical simulations of oscillatory flow through two-dimensional porous media configurations were performed by Graham & Higdon (2002), Iervolino *et al.* (2010) and Kardgar & Jafarian (2021). In our upcoming work (Unglehrt & Manhart, 2022), the onset of nonlinear effects was investigated in laminar oscillatory flow through a hexagonal sphere pack by numerical simulation.

The flow state in oscillatory flow depends on two dimensionless parameters: the Hagen number $Hg$ representing the amplitude and the Womersley number $Wo$ representing the frequency of the forcing. The Reynolds number $Re$ is a unique function of the Hagen and Womersley number. Therefore, either of Hagen or Reynolds number can be used to characterise the flow state. Based on a model equation, Gu & Wang (1991) estimated which flow regime might be expected for a given combination of $Re$ and $Wo$.

In the present contribution, we investigate the onset of turbulence in oscillatory flow through an idealised porous medium geometry by means of direct numerical simulation. A visual inspection of the instantaneous velocity fields suggests that the simulation database includes both laminar and turbulent simulations. However, it is unclear how to objectively quantify the flow state. Commonly, turbulence is characterised by temporal and spatial properties of the velocity fluctuations about the mean, e.g. the frequency or wavenumber spectra or the spatial two-point correlations. In the present case, the definition of a fluctuation is not trivial since the flow is unsteady and inhomogeneous in all spatial directions. One could perform a phase-dependent time average, but this comes at a large computational expense since the flow needs to be integrated over many cycles. As our objective is to merely differentiate between laminar and turbulent flow, we consider this cost to be disproportionate. On the other hand, especially at higher Womersley numbers analyses of the full velocity have the problem that the mean flow does not vary slowly compared to the turbulence and that the boundary and shear layers are not large compared to the turbulent scales. Therefore, the objective of the present work is to find quantitative evidence that allows to discern the laminar and the turbulent flow state.

First, we investigate the behaviour of the streamwise and cross-streamwise components of the superficial volume-averaged velocity. Second, we analyse the breaking of the symmetries that are imposed onto the flow by the sphere pack geometry. Third, we propose to average the flow over an ensemble of realisations that is generated using the symmetries

of the sphere pack geometry. This allows us to separate the velocity fields into an average and fluctuating part based on which we can distinguish laminar, transitional and turbulent cases.

## METHODOLOGY

### Numerical method

We performed direct numerical simulation of the incompressible Navier-Stokes equations with our in-house code MGLET that is based on Cartesian block-structured grids. The spatial discretisation in MGLET uses a second-order central finite volume scheme with a staggered arrangement of variables and the temporal discretisation employs a third-order explicit Runge-Kutta method. The no-slip boundary conditions on the spheres is enforced by a discrete-forcing immersed boundary method that is described in Peller *et al.* (2006); Peller (2010). The momentum fluxes near the immersed boundary are evaluated using a linear least-squares ghost-cell interpolation/extrapolation approach. The conservation of mass is enforced in every substep of the time integration scheme using a flux correction procedure in the interface cells and by solving a Poisson equation for a correction pressure in the field.

### Study design

As a porous medium, we choose a hexagonal close-packed arrangement of spheres of diameter $d$. It has a porosity of 0.259 which is the lower limit for packings of equal spheres. The flow is described by the incompressible Navier-Stokes equations with an an oscillatory volume force $f_x \sin \Omega t$ in the $x$–direction. Initially, the flow is at rest.

The problem is governed by two independent parameters: the Hagen number $Hg = f_x d^3/(\rho \nu^2)$ represents the ratio of the amplitude of the applied volume force to the viscous forces and the Womersley number $Wo = \sqrt{\Omega d^2/\nu}$ represents the ratio of the sphere diameter to the thickness of the oscillatory Stokes boundary layer. The Reynolds number $Re$ is based on the sphere diameter $d$ and the amplitude of the superficial volume-averaged velocity after the decay of the transient. The superficial velocity is defined as

$$\langle u \rangle_\mathrm{s} := \frac{1}{V} \int_{V_\mathrm{f}} u \, \mathrm{d}V$$

with the fluid volume $V_\mathrm{f}$ and the total volume $V$.

We consider flow at a Womersley number of 31.62 and four values of the Hagen number. In linear flow, the selected value of the Womersley number lies at the transition between the low and the high frequency regime that are governed by Stokes flow and potential flow, respectively. Consequently, our simulations belong to the mid frequency (MF) regime. The simulation parameters are reported in table 1.

### Domain size and grid spacing

The simulation domain consists of two unit cells in the $x$–direction and one unit cell in the $y$- and $z$–direction. It thus has an extent $2d \times \sqrt{3}d \times 2\sqrt{6}/3\,d$. For this size, the domain contains two spheres in every lattice direction. He *et al.* (2019) used a domain of the same volume for their direct numerical simulations of turbulent flow in a face-centred cubic sphere pack. They state that "the unit cell domain showed little variation in statistics compared to a larger domain".

Table 1: Simulation parameters.

| case | $Hg$ | $Wo$ | $Re$ | number of cycles |
|---|---|---|---|---|
| MF3 | $10^{5.5}$ | 31.62 | 26.9 | 3[†] |
| MF4 | $10^{6}$ | 31.62 | 74.0 | 4[†] / 1.32[‡] |
| MF5 | $10^{6.5}$ | 31.62 | 157 | 6.3975 |
| MF6 | $10^{7}$ | 31.62 | 297 | 1.63 |

[†] These simulations are presented in (Unglehrt & Manhart, 2022).

[‡] This simulation was recomputed with a more finely resolved triangle representation of the sphere pack geometry to match the other simulations.

The flow was computed with grid resolutions of 48, 96, 192 and 384 cells per diameter (cpd), resulting in a total number of 88 million fluid cells at 384 cpd. The error of the numerical solution was estimated based on the space-time $L^2$-norm of the velocity and on the oscillation amplitude of the superficial velocity $\langle u \rangle_\mathrm{s}$ which is used to form the Reynolds number. For all simulations the relative difference between the finest and the second finest resolution is less than 1.3%.

The resolution requirements come from the wall boundary layers and possibly the turbulence in the bulk. The characteristic thickness of the oscillatory boundary layer can be estimated as $\delta = \sqrt{2\nu/\Omega}$ which we resolve with 17 cells. On the other hand, He *et al.* (2019) employed a grid resolution of 250 (cpd) to simulate stationary turbulent flow up to $Re = 741$.

## RESULTS

### Instantaneous velocity fields

Figure 1a–d displays a section through the velocity field perpendicular to the main flow direction for our simulations. As the Hagen number is increased by powers of $\sqrt{10}$, the velocity field develops pronounced flow structures in the large pores, resembling those in transient flow described by Sakai & Manhart (2020). Due to the regular layout of the structures, we would consider the cases MF3–MF5 as laminar. At the highest Reynolds number, the velocity field is asymmetrical and irregular vortical structures can be made out. Intuitively, we would consider the case MF6 (figure 1d) as turbulent. In the following, we discuss quantitative evidence that allows us to objectively decide on the flow state.

### Superficial velocity

In this section, we discuss the behaviour of the superficial velocity as the flow state changes from laminar to (presumably) turbulent. The time series of the streamwise superficial velocity (figure 1e–h) remains relatively smooth throughout the changes in the velocity field. This is in contrast to the stationary case for which Hill & Koch (2002) and Sakai & Manhart (2020) reported (quasi-) periodic or chaotic oscillations of the streamwise superficial velocity. At the lowest Reynolds number, $\langle u \rangle_\mathrm{s}$ has a time lag with respect to the forcing and the amplitude is 25% below the steady state amplitude. As the Reynolds number is increased, the phase lag reduces and the peak amplitude approaches the steady state value that would be attained for the same Hagen number. At the highest Reynolds number, we observe a plateau rather than a pronounced peak.

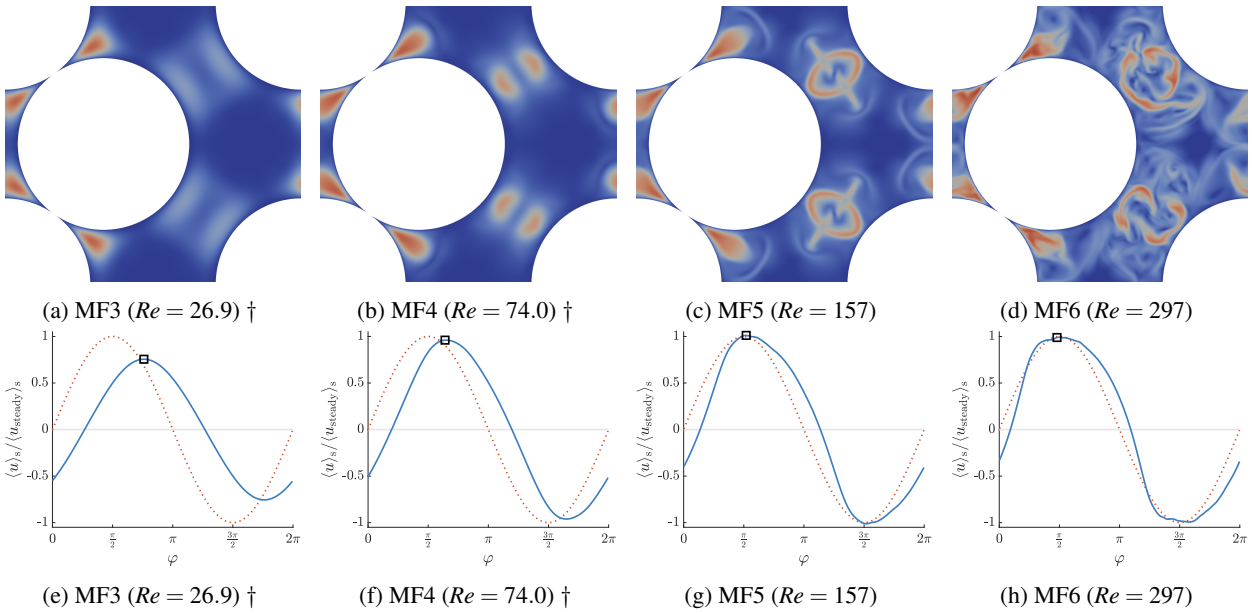


† simulations from (Unglehrt & Manhart, 2022)

Figure 1: (a)–(d) Velocity magnitude in the $y$-$z$-plane perpendicular to the flow direction. The velocity fields correspond to the time of the maximum superficial velocity. (e)–(f) Forcing (dotted red line) and superficial velocity (blue line) over one period. The superficial velocity is normalised with the steady state value (i.e. for a constant pressure gradient) obtained from the amplitude of the forcing via the relations given by Sakai & Manhart (2020). The black symbol marks the time of the snapshot presented in (a)–(d).

The cross-streamwise components of the superficial velocity, $\langle v \rangle_s$ and $\langle w \rangle_s$, are orthogonal to the imposed volume force. For the cases MF3 and MF4, these components are very small as a consequence of the symmetries of the sphere pack imprinted on the flow. On the other hand, for the cases MF5 and MF6 significant nonzero values of the cross-streamwise components can be observed. Figure 2 shows a plot of $\langle v \rangle_s$ and $\langle w \rangle_s$ for the latter simulations. The curves start out at the origin and spread out into the plane. For the case MF5, the amplitude of $\langle v \rangle_s$ is approximately 30 times larger than the amplitude of $\langle w \rangle_s$ and approximately 400 times smaller than the amplitude of $\langle u \rangle_s$. A clustering of points at the origin indicates that the cross-streamwise components grow in time. For the case MF6, the amplitude of $\langle v \rangle_s$ and $\langle w \rangle_s$ is approximately 60 times smaller than the amplitude of $\langle u \rangle_s$. Both cases shown in figure 2 exhibit irregular orbits, indicating chaotic behaviour. Moreover, the cross-streamwise components of the superficial velocity are only weakly correlated with the streamwise superficial velocity (represented by the colour of the curves).

While for MF6 the observed chaotic behaviour of the cross-streamwise components is in line with irregular structure of the velocity field shown in figure 1d, the visual impression of the velocity field of the case MF5 (figure 1c) does not suggest any chaotic behaviour in this case. This could be explained with the relatively low magnitude of the cross-streamwise components.

In conclusion, the streamwise superficial velocity changes gradually with Reynolds number and we could not identify features in the time series that could be used to clearly discern laminar and turbulent flow. Suprisingly, for higher Reynolds numbers the time and value of the maximum $\langle u \rangle_s$ coincide with the results of a quasi-steady approximation. On the other hand, the cross-streamwise components are very small for the cases MF3 and MF4 whereas they are nonzero and exhibit chaotic behaviour for MF5 and MF6.

## Quantification of symmetry breaking

In this section, we investigate the symmetry breaking of the flow which was already indicated by the cross-streamwise components of the superficial velocity.[1] Based on the works of Hill & Koch (2002) and Sakai & Manhart (2020), the symmetry breaking can be considered a prerequisite of turbulent flow in the sphere pack.

When a forcing is applied along the $x$–direction, laminar flow through the hexagonal sphere pack exhibits four symmetries: the flow is invariant with respect to

1. a translation by $d$ in the $x$–direction ($\mathscr{T}_x$)
2. a translation by $d$ at a 60° angle to the $x$–direction ($\mathscr{T}_{xy}$)
3. a reflection around $z = \sqrt{6}/3\,d$ ($\mathscr{S}_z$)
4. a rotation by $\pi$ about the axis $y = \sqrt{3}/3$, $z = \sqrt{6}/6$ ($\mathscr{R}_x$)

Figure 3 displays the result of these transformations applied to the sphere pack inside the simulation domain. Considering the periodic boundary conditions of the domain, the original and the transformed configurations of the spheres are congruent.

In order to investigate the possible breaking of these symmetries, we decompose the instantaneous velocity fields into a component $\mathbf{u}_{sym}$ that is symmetric with respect to one of the symmetries, and a corresponding antisymmetric component $\mathbf{u}_{anti}$. The kinetic energy of the antisymmetric component, $\langle k_{anti} \rangle_s = \left\langle \frac{1}{2} \rho \mathbf{u}_{anti}^2 \right\rangle_s$, measures the violation of the symmetry under consideration. Figure 4 displays the temporal evolution of $\langle k_{anti} \rangle_s$ for the various symmetries. For the cases MF3 and MF4 we observe that all symmetries are satisfied to an accuracy of more than $10^{-7}$. The amplitude of the antisymmetric components remains stationary. This indicates that the flow

[1] Please note the following connection between the symmetries and the cross-streamwise components of the superficial velocity: If the flow is symmetric under the rotation $\mathscr{R}_x$, then $\langle v \rangle_s = \langle w \rangle_s = 0$ and if the flow is symmetric under the reflection $\mathscr{S}_z$, then $\langle w \rangle_s = 0$.

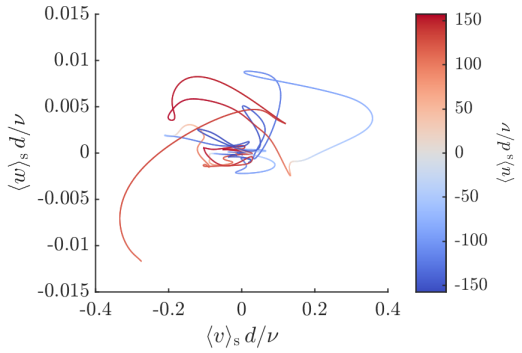


(a) MF5 ($Re = 157$)

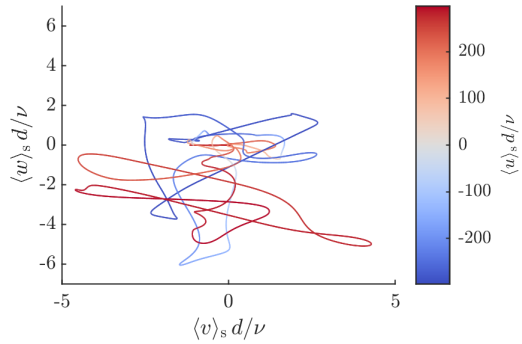


(b) MF6 ($Re = 297$)

Figure 2: Cross-streamwise components of the superficial velocity; the curves are coloured by the streamwise component of the superficial velocity. The irregular orbits indicate chaotic flow.

is stable with respect to the symmetry breaking and supports the hypothesis that the flow is laminar in these cases. For the case MF5 a simultaneous exponential growth of the energy of all antisymmetric components can be observed. After approximately 5 cycles, the kinetic energy of the $\mathscr{R}_x$-antisymmetric part saturates at 0.3% of the maximum total kinetic energy (cf. figure 4d). This suggests that (i) there exists a linear instability mechanism that facilitates the growth of the antisymmetric part and (ii) a nonlinear self-interaction of the instability occurs which limits its growth. However, this does not necessarily imply that the flow becomes turbulent. Finally, for the case MF6 a fast growth of the antisymmetric components can be observed. The kinetic energy of the antisymmetric components with respect to $\mathscr{R}_x$, $\mathscr{S}_z$ and $\mathscr{T}_{xy}$ peaks between 9 and 10% of the cycle maximum of the total kinetic energy.

The initial values of $\langle k_{\text{anti}} \rangle_s$ turned out to depend on the accuracy of the triangle representation of the spheres, from which the interpolation stencils and coefficients in the immersed boundary method are generated. There exist two sources of the initial symmetry breaking perturbations in our code: asymmetric interpolants at the immersed boundary and the residual of the pressure correction. A visual inspection of the antisymmetric parts of the velocity field shows that only the physically meaningful parts of these perturbations are amplified.

## Symmetry group averaging

In the preceding sections, it was demonstrated that the antisymmetric components of the velocity field show unsta-

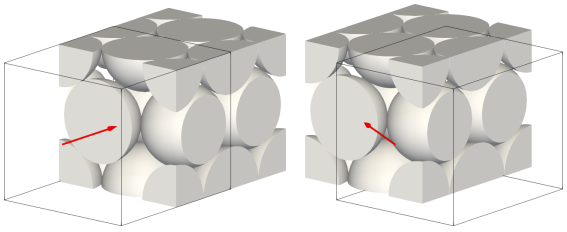

(a) Translation $\mathscr{T}_x$ (b) Translation $\mathscr{T}_{xy}$

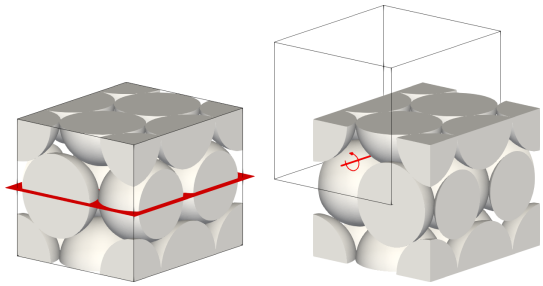

(c) Reflection $\mathscr{S}_z$ (d) Two-fold rotation $\mathscr{R}_x$

Figure 3: Symmetries of laminar flow in a hexagonal sphere pack due to a volume force along the $x$–direction. The black box represents the position of the sphere pack before the application of the symmetry operation.

ble or chaotic dynamics at $Re = 157$ and $Re = 297$. A direct inspection of the spatial distribution of the antisymmetric components is however not informative as in general, turbulent motion is neither symmetric nor antisymmetric. On the other hand, the mean velocity field of a turbulent flow is usually symmetric. Therefore, we decompose the velocity field into a part that satisfies all of the symmetries

$$\overline{\mathbf{u}} = \frac{1}{16} (\mathscr{I} + \mathscr{R}_x)(\mathscr{I} + \mathscr{T}_x)(\mathscr{I} + \mathscr{T}_{xy})(\mathscr{I} + \mathscr{S}_z)\mathbf{u} \qquad (1)$$

where $\mathscr{I}$ is the identity, and a residual component $\mathbf{u}' = \mathbf{u} - \overline{\mathbf{u}}$ which is in general neither symmetric nor antisymmetric with respect to any symmetry.

Alternatively, this decomposition can be interpreted as an average over the ensemble of 16 velocity fields that is generated by the action of the symmetry group. Such a symmetry average was used by Sirovich (1987); Sirovich & Park (1990) to enlarge the sample size for a proper orthogonal decomposition. Please note that while equation (1) can be understood as an ensemble average, it may not converge to the same result as a time or phase average. For example, Srikanth *et al.* (2021) investigated a persistent symmetry breaking phenomenon in a porous medium for which the time-averaged flow is asymmetrical. As there is an equal probability for the flow to deviate to either side, the ensemble mean flow would be symmetrical.

The symmetry group average (1) underestimates the energy of the turbulent fluctuations compared to the ensemble mean. This can be demonstrated as follows. As the flow problem is symmetric, the ensemble mean $E[\mathbf{u}]$ is symmetric and invariant with respect to $\mathscr{R}_x$, $\mathscr{T}_x$, $\mathscr{T}_{xy}$ and $\mathscr{S}_z$. For example, $\mathscr{R}_x E[\mathbf{u}] = E[\mathbf{u}]$ and $E[\mathscr{R}_x \mathbf{u}] = E[\mathbf{u}]$. Hence, the ensemble mean does not change under the symmetry group average, i.e. $\overline{E[\mathbf{u}]} = E[\mathbf{u}]$ and $E[\overline{\mathbf{u}}] = E[\mathbf{u}]$, and the expectation of the fluctuation about the symmetry group average is zero, i.e. $E[\mathbf{u}'] = E[\mathbf{u} - \overline{\mathbf{u}}] = 0$. Therefore $\mathbf{u}'$ is a part of the fluctuation about the ensemble mean.

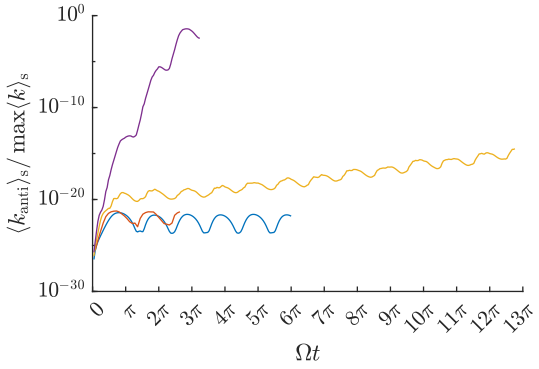


(a) Translation $\mathscr{T}_x$

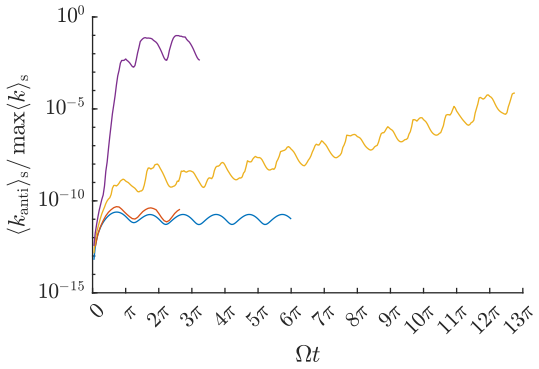


(b) Translation $\mathscr{T}_{xy}$

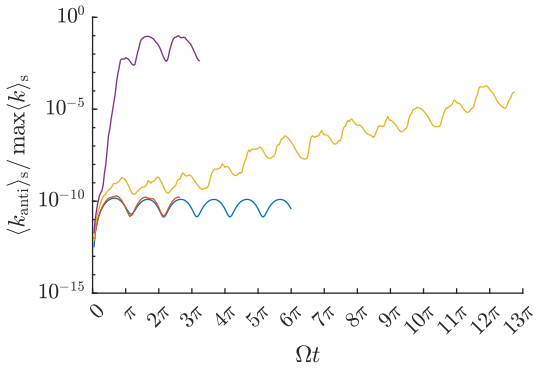


(c) Reflection $\mathscr{S}_z$

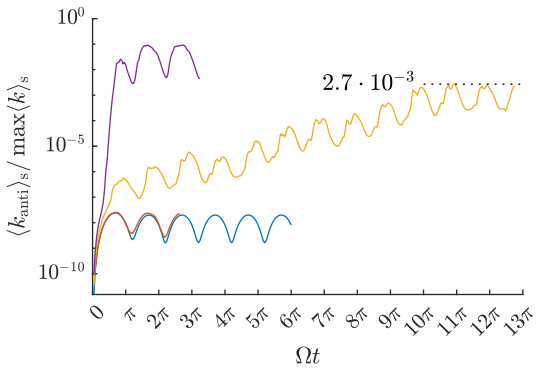


(d) Two-fold rotation $\mathscr{R}_x$

Figure 4: Volume-averaged kinetic energy of the antisymmetric components. — MF3 ($Re = 26.9$), — MF4 ($Re = 74.0$), — MF5 ($Re = 157$), and — MF6 ($Re = 297$). The kinetic energy $\langle k_{\mathrm{anti}}\rangle_{\mathrm{s}}$ is normalised with the maximum total kinetic energy of the last cycle.

Figure 5 displays the spatial distribution of the magnitude of $\overline{\mathbf{u}}$ and $\mathbf{u}'$. For the case MF5 the symmetry group averaged velocity field $\overline{\mathbf{u}}$ looks identical to the instantaneous field in figure 1c. This is due to the low energy of the antisymmetric components (cf. figure 4). The residual component $\mathbf{u}'$ features symmetric patterns that are arranged near the high-velocity features in $\overline{\mathbf{u}}$. For the case MF6, the symmetry group averaged velocity field contains symmetric versions of the high-intensity regions near the contact points and inside the large pores that can be identified in figure 1d. The residual velocity field $\mathbf{u}'$ does not contain these features; instead many irregular and small scale vortices can be identified.

## CONCLUSION

We performed direct numerical simulation of oscillatory flow through a hexagonal sphere pack at $Wo = 31.62$ and four Reynolds numbers. We investigated instantaneous velocity fields, the time series of the streamwise and cross-streamwise superficial velocity and the breaking of the symmetries of the flow. Moreover, the velocity field was averaged over the ensemble of realisations generated from the instantaneous velocity fields by applying the symmetries of the sphere pack, and the spatial distributions of the average and fluctuation field were discussed. The resulting average field approximates the ensemble mean of the flow and the resulting fluctuations are a subset of the fluctuations about the ensemble mean.

At $Re = 26.9$ and $Re = 74.0$ the cross-streamwise components of the superficial velocity are nearly zero and the flow shares all symmetries of the sphere pack. Consequently, these cases can be considered as laminar. On the other hand, the symmetries of the flow are broken for $Re = 157$ and $Re = 297$ and the cross-streamwise superficial velocity show nonzero values and chaotic behaviour. At $Re = 157$ the antisymmetric parts of the velocity field with respect to the symmetries of the sphere pack grow exponentially in time, indicating that a linear instability is present in the flow. Eventually, the antisymmetric part with respect to the rotation symmetry (cf. figure 3d) saturates at 0.3% of the total kinetic energy and a similar behaviour could be expected for the other symmetries. The fluctuations with respect to the symmetry group average have an ordered appearance, corroborating that this flow case is not yet turbulent. Consequently, we categorise it as a transitional flow. Finally, at $Re = 297$ the symmetries are broken rapidly and the antisymmetric parts of the velocity field peak at approximately 10% of the total kinetic energy. The fluctuations about the symmetry group average consist of disorderd vortical structures and a scale separation can be observed between the fluctuating and the average field. Together with the chaotic behaviour of the cross-streamwise superficial velocity, this strongly supports the view that this case exhibits turbulent flow.

Further investigations may be necessary to assess the effect of the domain size and the dependency of the results on the Womersley number. Moreover, our findings for the case at $Re = 157$ suggest that a Floquet-type linear instability analysis of the flow could be interesting.

## ACKNOWLEDGEMENTS

The authors gratefully acknowledge the financial support of the DFG under grant no. MA2062/13-1. Computing time was granted by the Leibniz Supercomputing Centre on its Linux-Cluster.

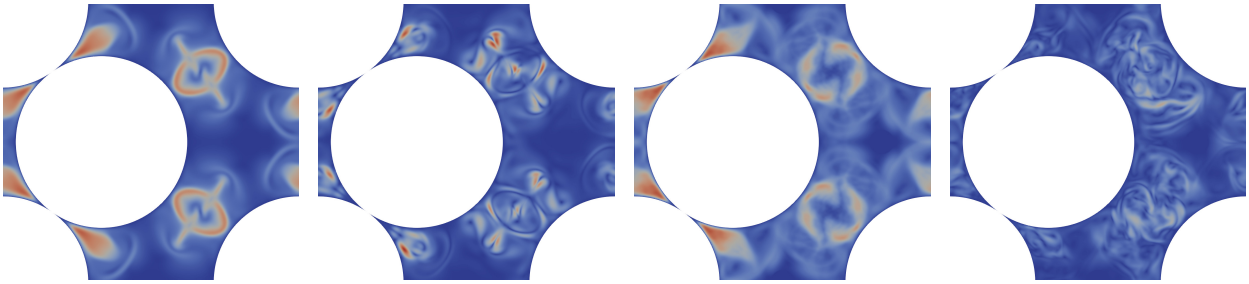

(a) $|\overline{\mathbf{u}}|$ for MF5 ($Re = 157$) (b) $30\,|\mathbf{u}'|$ for MF5 ($Re = 157$) (c) $|\overline{\mathbf{u}}|$ for MF6 ($Re = 297$) (d) $|\mathbf{u}'|$ for MF6 ($Re = 297$)

Figure 5: Magnitude of the symmetry group average velocity $\overline{\mathbf{u}}$ and the corresponding fluctuation $\mathbf{u}'$ in the $y$-$z$-plane perpendicular to the flow direction. The velocity fields correspond to figure 1c–d.

## REFERENCES


Bağcı, Ö., Arbak, A., De Paepe, M. & Dukhan, N. 2016 Experimental results for oscillatory water flow in 10-ppi metal foam at low-frequencies. *Journal of Physics: Conference Series* **745**, 032040.

Crittenden, B. D., Lau, A., Brinkmann, T. & Field, R. W. 2005 Oscillatory flow and axial dispersion in packed beds of spheres. *Chemical Engineering Science* **60** (1), 111–122.

Dybbs, A. & Edwards, R. V. 1984 A New Look at Porous Media Fluid Mechanics — Darcy to Turbulent. In *Fundamentals of Transport Phenomena in Porous Media* (ed. J. Bear & M. Y. Corapcioglu), *NATO ASI Series*, vol. 82, pp. 199–256. Dordrecht: Springer Netherlands.

Fand, R. M., Kim, B. Y. K., Lam, A. C. C. & Phan, R. T. 1987 Resistance to the Flow of Fluids Through Simple and Complex Porous Media Whose Matrices Are Composed of Randomly Packed Spheres. *Journal of Fluids Engineering* **109** (3), 268–273.

Graham, D. R. & Higdon, J. J. L. 2002 Oscillatory forcing of flow through porous media. Part 2. Unsteady flow. *Journal of Fluid Mechanics* **465**.

Gu, Z. & Wang, H. 1991 Gravity waves over porous bottoms. *Coastal Engineering* **15** (5-6), 497–524.

Hall, K. R., Smith, G. M. & Turcke, D. J. 1995 Comparison of oscillatory and stationary flow through porous media. *Coastal Engineering* **24** (3-4), 217–232.

He, X., Apte, S. V., Finn, J. R. & Wood, B. D. 2019 Characteristics of turbulence in a face-centred cubic porous unit cell. *Journal of Fluid Mechanics* **873**, 608–645.

Hill, R. J. & Koch, D. L. 2002 The transition from steady to weakly turbulent flow in a close-packed ordered array of spheres. *Journal of Fluid Mechanics* **465**, 59–97.

Iervolino, M., Manna, M. & Vacca, A. 2010 Pulsating Flow through Porous Media. In *Turbulence and Interactions* (ed. E. H. Hirschel, W. Schröder, K. Fujii, W. Haase, B. Leer, M. A. Leschziner, M. Pandolfi, J. Periaux, A. Rizzi, B. Roux, Y. I. Shokin, M. Deville, T.-H. Lê & P. Sagaut), , vol. 110, pp. 167–173. Berlin, Heidelberg: Springer Berlin Heidelberg.

Kardgar, A. & Jafarian, A. 2021 Numerical simulation of turbulent oscillating flow in porous media. *Scientia Iranica* **28** (2), 743–756.

Losada, I. J., Losada, M. A. & Martín, F. L. 1995 Experimental study of wave-induced flow in a porous structure. *Coastal Engineering* **26** (1-2), 77–98.

Lowe, R. J., Shavit, U., Falter, James L., Koseff, J. R. & Monismith, S. G. 2008 Modeling flow in coral communities with and without waves: A synthesis of porous media and canopy flow approaches. *Limnology and Oceanography* **53** (6), 2668–2680.

Pamuk, M. T. & Özdemir, M. 2014 Hydrodynamic Aspects of Oscillating Flow Through Porous Media Consisting of Steel Spheres. In *Progress in Exergy, Energy, and the Environment* (ed. I. Dincer, A. Midilli & H. Kucuk), pp. 633–640. Cham: Springer International Publishing.

Patil, V. A. & Liburdy, J. A. 2012 Flow Structure Identification in Unsteady Flow in Porous Media. In *Proceedings of the Asme Fluids Engineering Division Summer Meeting, 2012, Vol 1, Pts a and B, Symposia*, pp. 775–781. New York: Amer Soc Mechanical Engineers.

Patil, V. A. & Liburdy, J. A. 2013 Flow structures and their contribution to turbulent dispersion in a randomly packed porous bed based on particle image velocimetry measurements. *Physics of Fluids* **25** (11), 113303.

Peller, N. 2010 Numerische Simulation turbulenter Strömungen mit Immersed Boundaries. PhD thesis, Technische Universität München, München.

Peller, N., Le Duc, A., Tremblay, F. & Manhart, M. 2006 High-order stable interpolations for immersed boundary methods. *International Journal for Numerical Methods in Fluids* **52** (11), 1175–1193.

Sakai, Y. & Manhart, M. 2020 Consistent Flow Structure Evolution in Accelerating Flow Through Hexagonal Sphere Pack. *Flow, Turbulence and Combustion* **105** (2), 581–606.

Shigematsu, T., Nakajo, S. & Okada, Y. 2018 An experimental study on the interaction between oscillatory flow and idealized porous bed. *Journal of Coastal Research* pp. 981–985.

Sirovich, L. 1987 Turbulence and the Dynamics of Coherent Structures Part II: Symmetries and Transformations. *Quarterly of Applied Mathematics* **XLV**, 573–82.

Sirovich, L. & Park, H. 1990 Turbulent thermal convection in a finite domain: Part I. Theory. *Physics of Fluids A: Fluid Dynamics* **2** (9), 1649–1658.

Srikanth, V., Huang, C.-W., Su, Timothy S. & Kuznetsov, A. V. 2021 Symmetry breaking of turbulent flow in porous media composed of periodically arranged solid obstacles. *Journal of Fluid Mechanics* **929**.

Unglehrt, L. & Manhart, M. 2022 Onset of nonlinearity in oscillatory flow through a hexagonal sphere pack. *Submitted to Journal of Fluid Mechanics*.

van Gent, M. R. A. 1993 Stationary and oscillatory flow through coarse porous media. *Communications on hydraulic and geotechnical engineering, No. 1993-09* .